SAND2021-14618C

Integrated power converters for optimal operation of Hybrid battery packs

Oindrilla Dutta, Jacob Mueller, Robert Wauneka, Valerio De Angelis, and David Rosewater, *Members, IEEE*
Sandia National Laboratories, Albuquerque, NM 87185
email: odutta@sandia.gov, jmuelle@sandia.gov, rwaunek@sandia.gov, vdeange@sandia.gov, and dmrose@sandia.gov

***Abstract*—This work demonstrates a method to build and operate hybrid battery systems, which can serve the need for Long-Duration Energy Storage (LDES). LDES systems have to provide energy at different timescales to compensate for the intermittency of renewable resources, supply peak power, support black-start, and serve loads with variable power factor. It is cost prohibitive to use a single battery technology to provide both high power and energy services. Therefore, integration of hybrid technologies is essential. Here, a scalable and flexible method is proposed to build such a hybrid system, where DC-DC converters are integrated between battery packs and a DC-AC converter. The DC-DC converters implement battery-specific charging/discharging protocols, and the DC-AC converter establishes the DC bus voltage and synchronizes with the grid. A hardware-software testbed has been built for operating Lead-Acid battery cells by integrating a commercial DC-AC power conversion system (PCS) with a custom-built Dual Active Bridge (DAB) DC-DC converter. The results validate this method's effectiveness in controlling hybrid battery strings and preventing battery degradation. The authors plan to make the software and hardware design available to the power electronics and battery community, and add support for other DC-DC converter topologies and battery technologies.**

***Index Terms*—DAB, DC-AC converters, hybrid batteries.**

I. Introduction

Easy implementation and testing of battery energy storage systems (BESSs) are essential to facilitate renewable integration. BESSs are required to operate for different time spans to provide reliability, stability, and resiliency. Several battery technologies are used in grid applications, such as Pb-Acid, Li-ion, NiCd, VRB, NaS, $ZnBr_2$, regenerative fuel cell, and metal air [1]–[3]. However, a single battery technology cannot support all the grid functionalities. Pb-Acid batteries are extensively used for their low capital cost and wide availability. However, they are heavy, with low energy density, and short life span of < 500 cycles [4]. Li-ion batteries have high efficiency, energy, and power-densities. However, they are expensive, and can degrade quickly if utilized at a high depth of discharge [5] or improperly charged. NaS batteries have excellent pulse-power capability, but are expensive and have high operating temperature. VRB batteries can provide long-duration storage services, but are slow to ramp up. The widely varying benefits/drawbacks of different battery technologies makes Hybrid Energy Storage Systems (HESSs) necessary to support the power grid with flexible energy storage systems.

The applications of HESSs have been extensively studied [6]. Three types of connection topology, viz. passive, semi-active, and active, have been proposed. In passive topology the HESSs are directly connected to each other and form the DC bus, which is tied to the grid through a DC-AC converter. In semi-active mode, a DC-DC converter is connected between a high power storage (like a capacitor bank) and a DC-AC converter, whereas the high energy storage is directly connected to the DC-AC converter. In active topology, DC-DC converters are integrated between a DC-AC converter and all the HESSs. Most demonstration projects have implemented the passive topology [7]–[10]. This topology offers a low degree of control and cannot accommodate different battery cycling methods. It also fails to handle the high range of voltage variation across the different technologies, which regularly occurs during charge-discharge and increases as batteries age. Also, replacement and maintenance of a single battery string can only be performed by completely disabling the entire system. Finally, commercial single phase PCSs, which are popular for their low-cost, introduce ripples at the DC bus. This may cause considerable acceleration of battery aging [11]–[14]. The active HESS topology could accommodate different charge/discharge procedures for each type of batteries, and has been adopted in literature [15]–[19]. However, a practical example of an active HESS topology is only found in electric vehicles, where the storage consists of Li-batteries and ultracapacitors (UCs). Li-ion batteries are used for a few hours ($\sim$250 miles) and UCs are used to handle acceleration and regenerative braking. Grid applications require energy storage to provide power reserve (hours to days), peak shaving (hours), load regulation (minutes to hours), and black-start support (down to milli-seconds). In fact, the trend is now to design Long-Duration Energy Storage (LDES) that can provide energy for more that 4-6 hours and up to days. Therefore, Li-batteries and UCs need to be complemented by other longer duration battery technologies. All these technologies operate in different voltage windows and cannot simply be directly connected on a DC bus. The alternative to connecting all these resources on the DC bus (which is currently done) increases costs and management complexities.

This work aims to provide an expandable and modular framework that is based on open-source software and a flexible DC-DC converter topology that can be used to build HESS with an active topology that accommodates any energy storage technology. The approach has been demonstrated using a hardware testbed for cycling strings of Pb-acid cells at different voltages by integrating a Dual Active Bridge (DAB) DC-DC converter with a commercial PCS. This initial system ad-

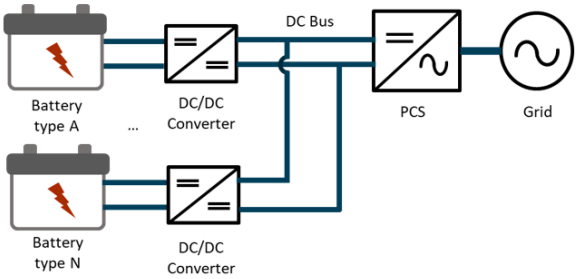

Fig. 1. Proposed system for connecting hybrid battery technologies for long duration energy storage in grid applications. The system relies on one AC/DC converters and still allows managing each type of battery independently.

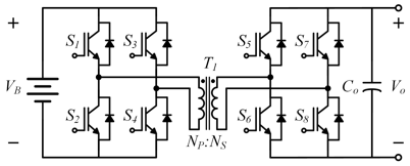

(a) Dual Active Bridge topology.

(b) DAB converter designed and built at Sandia National Labs.

Fig. 2. Dual Active Bridge (DAB) DC-DC Converter.

dresses the practical challenges of system integration, including coordination among the multiple control loops, monitoring of the different parameters without sample aliasing, alongside ease and safety of operation. The hardware set-up along with the control firmware can be expanded to accommodate other types of batteries and DC-DC converters.

II. Proposed System

This section describes our proposed method, shown in Fig. 1, where each type of battery is connected to a DC-DC DAB converter. These converters form a DC bus, where the DC-AC PCS integrates to the grid. In this work, the most widely used commercial PCS has been implemented in the test setup. This facilitates the use of existing commercial converters, instead of building a customized DC-AC converter.

A. Dual Active Bridge Converter

This section provides a brief overview of the DAB topology and the converter developed at the Advanced Power Electronic Conversion System laboratory (APEX) of Sandia National Labs (SNL), shown in Fig. 2. This topology provides the advantages of high power density, high switching frequency with soft switching, and galvanic isolation [20]. The power transfer, represented by (1), between the two bridges in the DAB is guided by the phase difference (ψ) between the primary (V_p) and secondary (V_s) voltages [21]. In this work,

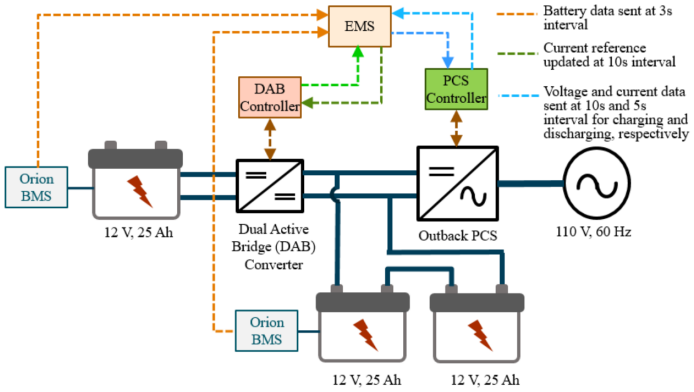

Fig. 3. Test set-up comprising battery packs, DAB DC-DC converter, Outback DC-AC converter, with their respective controllers and communication layer.

the DAB parameters have been designed for a nominal power of 75W with nominal V_p and V_s of 12 and 24V, respectively.

$$P_{DAB} = \frac{n_{tr} V_p V_s \psi(\pi - \psi)}{2\pi^2 f_{sw} L_{leak}} \quad (1)$$

B. Test Set-up

The test set-up comprising a hardware test bed and a communication layer, as shown in Fig. 3, is described here.

1) Hardware Test Bed: The hardware test bed, illustrated in Fig. 4, has been built for Pb-acid batteries, where each Pb-acid cell has a nominal voltage of 2V. 12 such cells, forming a 24V battery stack, have been connected to the high voltage (HV) side of the DAB converter. Another string of 12V, containing 6 cells, forms the low voltage (LV) side of the DAB. This DAB is integrated to a Outback PCS at the 24V DC link. The Outback PCS is connected to a regenerative grid emulator at the grid voltage and frequency of 120V and 60 Hz, respectively.

Each battery stack is provided with an Orion battery management systems (BMS) which provides cell voltage and string current measurements among other parameters. Monitoring and control of the DC-AC converter is performed by the PCS

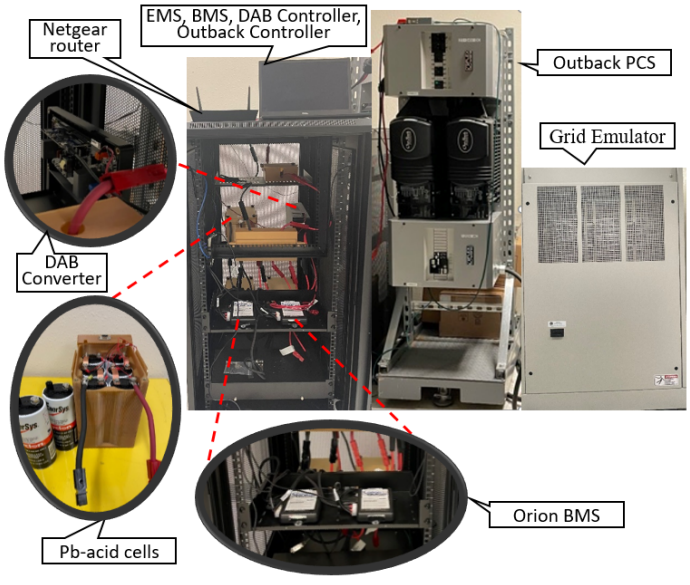

Fig. 4. Hardware test-bed comprising Pb-Acid battery packs, DAB DC-DC converter, Outback DC-AC converter, BMS, and system controllers.

Controller (PCS-C). Both the BMS and PCS-C communicate using the Sunspec Modbus interface specified by IEEE 1547-2018 [22]. The DAB Controller (DAB-C) is a C200 series microcontroller from TI, where a feedback control loop that modulates the phase-shift has been implemented. The EMS functions as a central controller, which receives monitoring signals from the BMS, PCS-C and DAB-C, based on which it regulates the charging/discharging operation of the batteries. Interoperability of the BMS, PCS-C, DAB-C and EMS are performed by an operator from a computer, to which the components are connected via the Netgear router.

2) Control Protocol : The sequence of control commands and monitoring signals are depicted in the flowchart in Fig. 5. The different sampling time for the four controllers, and assorted timestamps for data exchange are described below:

1) The EMS starts two parallel threads, viz. Battery and Inverter threads, which correspond to data to/from Orion BMSs and Outback PCS, respectively. These threads initialize a *battery* and an *inverter* object, which are shared with the Inverter and the Battery thread, respectively. Hence, the Inverter thread is started with a delay of 1s after initializing the battery thread. The *battery* object is used to obtain string currents $(I_{B-HV/LV})$, and cell voltages from which string voltages $(V_{B-HV/LV})$ are estimated. The *inverter* object provides DC voltage/current (V_{DC}/I_{DC}), and AC voltage/current (V_{AC}/I_{AC}). Prior to starting the two threads, charging/discharging current limits $(I_{ch/dis-lim})$ are specified in the PCS registers.
2) The EMS also starts a GUI that lets the operator set desired charging/discharging voltage (V_{ref}), which is sent to the PCS via the *inverter* object.
3) The *battery* object is sent to the EMS at an interval of 3s, whereas the *inverter* object is sent at 10s and 5s interval for charging and discharging, respectively. Determination of these time-steps are based on the speed at which data can be sent over the Modbus without congesting the communication channels, and is crucial for operating the integrated system reliably so that performance of all the constituents are synchronized.
4) According to the charging protocol for Pb-acid batteries, V_{ref} is set as the float voltage by the PCS-C, whereas the absorb and refloat voltages are set as $V_{ref} \pm \Delta V_{ch}$, respectively. For discharging, the PCS-C sets V_{ref} as sell voltage, and float voltage is specified as $V_{ref} + \Delta V_{dis}$.
5) If $V_{ref} > V_{B-HV}$, then the PCS-C is set to charge the battery on the HV side. A 1.5 minute moving average of I_{B-HV} is provided as I_{ref} to the DAB-C, which initiates charging on the LV side. I_{ref} is updated every 10s. Similarly, the PCS-C discharges when $V_{ref} < V_{B-HV}$. The DAB-C sends switching signals to the control card, based on I_{ref} and its feedback control loop.
6) This cycling process can be stopped/reset from the GUI.

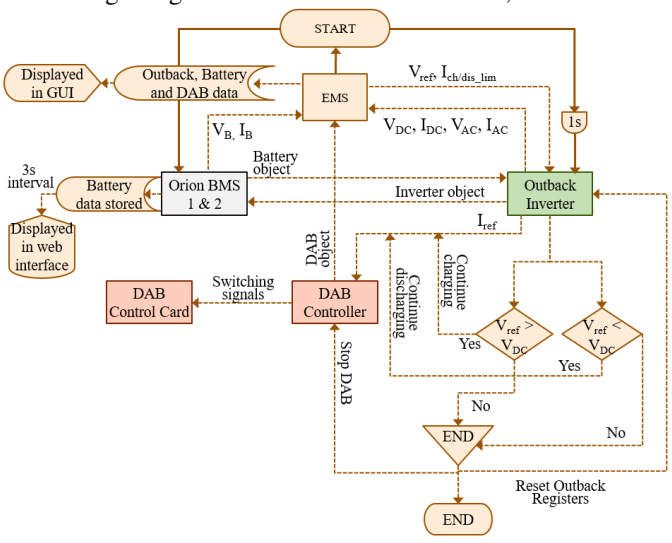

Fig. 5. Control flowchart consists of BMS, EMS, PCS, DAB Controllers.

III. Results & Discussion

The system in Fig. 4 has been used to cycle the 12V and 24V battery packs, with an objective of incorporating flexibility in the charge/discharge procedure so as to conform to the recommended principle of cycling Pb-acid batteries. The 24V battery pack represents the traditional solution adopted in most demonstration projects, and hence will be used to evaluate the performance of the existing topology, whereas the voltage and current profiles at the 12V battery pack will represent the potential of our proposed solution.

In a typical single phase AC-DC PCS, the DC bus is characterized by an AC ripple with a frequency equal to twice the line frequency [23]. As mentioned earlier, these ripples cause significant degradation of batteries, and Fig. 6 shows that existing commercial PCSs do not filter out these ripples. The charging current in Fig. 6a shows that the Outback PCS introduces a current ripple with a magnitude of 1.23A along with other noises at the 24V DC link. A zoomed in view showing I_{B-LV} and the 120Hz ripple at I_{B-HV} are illustrated in Fig. 6b. I_{B-LV} has a much smaller ripple with a frequency equal to the DAB switching frequency of 100 kHz, as shown in Fig. 6c. Thus, the DAB is able to filter out the 120 Hz ripples, thereby avoiding faster degradation of the 12V battery pack.

A similar experiment has been performed for discharging the batteries and the corresponding results are illustrated in Fig. 7. The impact of DC to AC conversion by an inverter on the DC side current is that the current is no longer a pure DC. It is characterized by a second harmonic component of the line frequency, along with other high switching-frequency components [23], as represented by (2).

$$i_{DC}(t) = \frac{v_{AC}(t) i_{AC}(t)}{V_{DC}} cos\phi - \frac{v_{AC}(t) i_{AC}(t)}{\sqrt{2} V_{DC}} cos(2\omega_{AC} t - \phi) \quad (2)$$

Fig. 7a demonstrates I_{B-LV} of the DAB, and the ripples introduced by the PCS on the 24V battery pack during discharging. A zoomed in view of I_{B-LV} in Fig. 7b shows that much smaller ripples, occurring at the DAB switching frequency of 100kHz, are introduced by the DAB on the 12V battery pack. Magnitude of the harmonics in I_{B-HV} during charging and discharging are shown in Figs. 8a and 8b, respectively, with a total harmonic distortion (THD) of 56.67% and 13.56%.

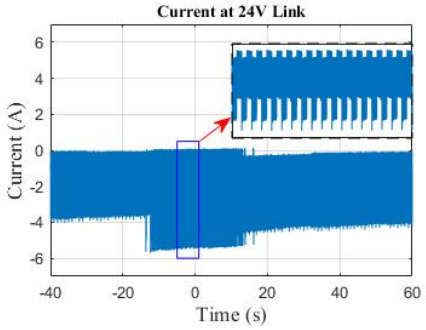

(a) Current at 24V DC link showing a noisy signal.

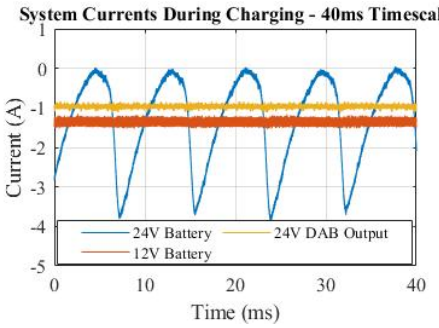

(b) Currents measured at millisecond time-scale

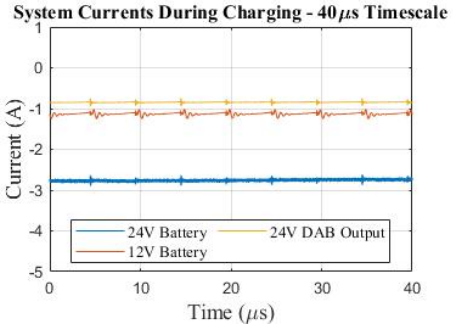

(c) Current measured at microsecond time-scale

Fig. 6. Charging current measured at three different points (24V DAB output, 24V, and 12V batteries) showing high magnitude ripples of 120Hz at 24V link and very low magnitude ripples of 100kHz at the 12V battery.

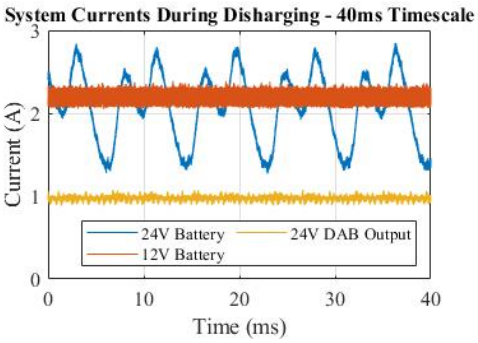

(a) Current measured at millisecond time-scale.

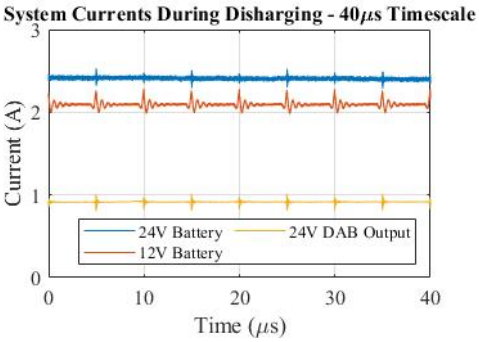

(b) Current measured at microsecond time-scale.

Fig. 7. Discharging current measured at three different points (24V DAB output, 24V, and 12V batteries) showing high magnitude ripples of ∼120Hz at 24V link and very low magnitude ripples of 100kHz at the 12V battery.

Alongside ripples, another limitation of traditional connections is the lack of flexibility in regulating the cycling of batteries. Hence, charge-discharge cycling of the Pb-acid battery packs have been performed following the control protocol in Section II-B2, where $I_{ch/dis-lim} = 3$ and 2 A; $V_{ref} = 25$ and 23.8 V; $\Delta V_{ch/dis} = 1.2$ and 0.2 V, respectively, for charging and discharging. A portion of this cycling is demonstrated in Fig. 9, where high magnitude ripples can be observed at the 24V DC link. However, the current and voltage at the LV side of the DAB contains very low magnitude ripples during both charge and discharge cycles. Besides, Fig. 9a shows that the LV battery can be disconnected ($I_{B-LV} = 0$), without making the entire system offline. This provides flexibility in situations where a specific battery string requires replacement/maintenance.

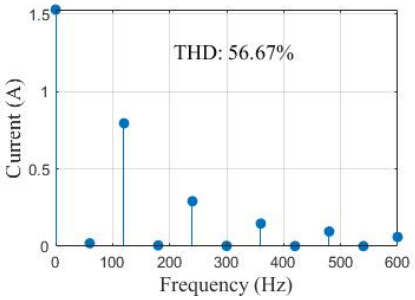

(a) Charging current at 24V battery pack.

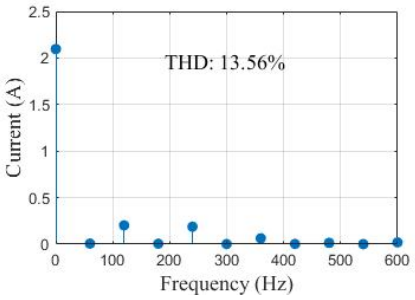

(b) Discharging current at 24V battery pack.

Fig. 8. Fourier analysis of the charging and discharging currents of the 24V battery pack showing a high percentage of total harmonic distortion.

IV. Conclusion and Future Work

This study proposed and demonstrated a method to facilitate the integration and testing of hybrid battery technologies. This method is based on integrating DC-DC converters between each battery pack and a DC-AC PCS. The DC-DC converters are responsible for implementing varying control protocols that are specific to the battery technologies. The PCS is responsible for establishing and regulating the DC bus voltage and also synchronizing with the grid.

A hardware testbed has been developed using a DAB DC-DC converter, a commercial DC-AC converter and Pb-acid battery packs. The control firmware for this testbed has been built using open source software, and is expandable to accommodate other battery technologies. This test-bed has been used to cycle two Pb-acid battery packs. A 24 V pack was directly connected to the DC-AC converter and a 12 V pack was connected on the low-voltage side of the the DAB. The high-voltage side of the DAB was connected in parallel with the 24 V pack and integrated to a commercial DC-

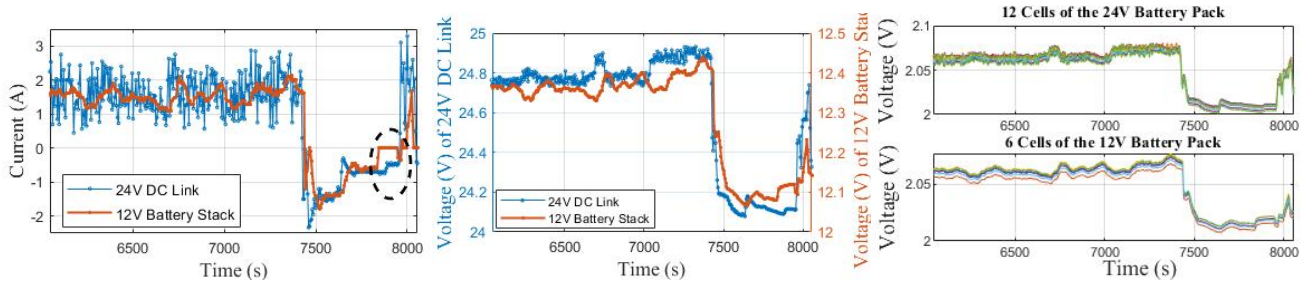

(a) String currents (b) String voltages (c) Cell voltages

Fig. 9. One charging and discharging cycle of the 24V and 12V battery packs showing high magnitude ripples at the 24V DC link, and smooth current as well as voltage at the 12V battery pack, along with selective disconnection of the 12V stack.

AC PCS. Experimental results show that the DAB accurately charges the 12V pack at the same rate at which the 24V pack is charged. In addition, the current and voltage of the high voltage (24V) battery show high magnitude ripples of 120 Hz, along with other noises during both charging (THD $= 56.67\%$) and discharging (THD $= 13.56\%$). However, the low voltage (12V) battery pack shows negligible ripples at the DAB switching frequency of 100 kHz. The results also show that the low voltage battery can be stopped (to be, for example, maintained or replaced) without disabling the entire system.

As part of the future work, the test set-up will be expanded to accommodate hybrid battery technologies and their specific control protocols. In addition, predictive cell degradation models will be used to adjust the charge protocol and voltage limits of each battery pack as the batteries age.

ACKNOWLEDGMENT

The authors would like to thank Dr. Imre Gyuk, Director of Energy Storage Research, for his guidance and support. Sandia National Laboratories is a multi-mission laboratory managed and operated by National Technology and Engineering Solutions of Sandia, LLC., a wholly owned subsidiary of Honeywell International, Inc., for the U.S. Department of Energy National Nuclear Security Administration under contract DE-NA-0003525.

REFERENCES

[1] K. Divya and J. Østergaard, "Battery energy storage technology for power systems—an overview," *Electric power systems research*, vol. 79, no. 4, pp. 511–520, 2009.

[2] X. Luo, J. Wang, M. Dooner, and J. Clarke, "Overview of current development in electrical energy storage technologies and the application potential in power system operation," *Applied energy*, vol. 137, pp. 511–536, 2015.

[3] M. Aneke and M. Wang, "Energy storage technologies and real life applications–a state of the art review," *Applied Energy*, vol. 179, pp. 350–377, 2016.

[4] H. Chen, T. N. Cong, W. Yang, C. Tan, Y. Li, and Y. Ding, "Progress in electrical energy storage system: A critical review," *Progress in natural science*, vol. 19, no. 3, pp. 291–312, 2009.

[5] I. E. Commission *et al.*, "Electrical energy storage: white paper," *Geneva, Switzerland: International Electrotechnical Commission*, pp. 1–78, 2011.

[6] T. S. Babu, K. R. Vasudevan, V. K. Ramachandaramurthy, S. B. Sani, S. Chemud, and R. M. Lajim, "A comprehensive review of hybrid energy storage systems: Converter topologies, control strategies and future prospects," *IEEE Access*, vol. 8, pp. 148 702–148 721, 2020.

[7] M. Koller and B. VöLlmin, "Preliminary findings of a 1 mw battery energy storage demonstration project," 2013.

[8] P. Lyons, N. Wade, T. Jiang, P. Taylor, F. Hashiesh, M. Michel, and D. Miller, "Design and analysis of electrical energy storage demonstration projects on uk distribution networks," *Applied Energy*, vol. 137, pp. 677–691, 2015.

[9] M. T. Lawder, B. Suthar, P. W. Northrop, S. De, C. M. Hoff, O. Leitermann, M. L. Crow, S. Santhanagopalan, and V. R. Subramanian, "Battery energy storage system (bess) and battery management system (bms) for grid-scale applications," *Proceedings of the IEEE*, vol. 102, no. 6, pp. 1014–1030, 2014.

[10] L. Yao, B. Yang, H. Cui, J. Zhuang, J. Ye, and J. Xue, "Challenges and progresses of energy storage technology and its application in power systems," *Journal of Modern Power Systems and Clean Energy*, vol. 4, no. 4, pp. 519–528, 2016.

[11] A. Bessman, R. Soares, O. Wallmark, P. Svens, and G. Lindbergh, "Aging effects of ac harmonics on lithium-ion cells," *Journal of Energy Storage*, vol. 21, pp. 741–749, 2019.

[12] S.-A. Amamra, Y. Tripathy, A. Barai, A. D. Moore, and J. Marco, "Electric vehicle battery performance investigation based on real world current harmonics," *Energies*, vol. 13, no. 2, p. 489, 2020.

[13] A. Ghassemi, P. C. Banerjee, Z. Zhang, A. Hollenkamp, and B. Bahrani, "Aging effects of twice line frequency ripple on lithium iron phosphate (lifepo 4) batteries," in *2019 21st European Conference on Power Electronics and Applications (EPE'19 ECCE Europe)*. IEEE, 2019, pp. P–1.

[14] F. Chang, F. Roemer, and M. Lienkamp, "Influence of current ripples in cascaded multilevel topologies on the aging of lithium batteries," *IEEE Transactions on Power Electronics*, vol. 35, no. 11, pp. 11 879–11 890, 2020.

[15] I. J. Cohen, D. A. Wetz, J. M. Heinzel, and Q. Dong, "Design and characterization of an actively controlled hybrid energy storage module for high-rate directed energy applications," *IEEE Transactions on Plasma Science*, vol. 43, no. 5, pp. 1427–1433, 2015.

[16] A. M. Gee, F. V. Robinson, and R. W. Dunn, "Analysis of battery lifetime extension in a small-scale wind-energy system using supercapacitors," *IEEE transactions on energy conversion*, vol. 28, no. 1, pp. 24–33, 2013.

[17] U. Manandhar, N. R. Tummuru, S. K. Kollimalla, A. Ukil, G. H. Beng, and K. Chaudhari, "Validation of faster joint control strategy for battery- and supercapacitor-based energy storage system," *IEEE Transactions on Industrial Electronics*, vol. 65, no. 4, pp. 3286–3295, 2017.

[18] S. K. Kollimalla, M. K. Mishra, A. Ukil, and H. B. Gooi, "Dc grid voltage regulation using new hess control strategy," *IEEE Transactions on Sustainable Energy*, vol. 8, no. 2, pp. 772–781, 2017.

[19] O. Dutta, M. Saleh, M. Khodaparastan, and A. Mohamed, "A dual-stage modeling and optimization framework for wayside energy storage in electric rail transit systems," *Energies*, vol. 13, no. 7, p. 1614, 2020.

[20] J. A. Mueller and J. W. Kimball, "Modeling dual active bridge converters in dc distribution systems," *IEEE Transactions on Power Electronics*, vol. 34, no. 6, pp. 5867–5879, 2019.

[21] B. Zhao, Q. Song, W. Liu, and Y. Sun, "Overview of dual-active-bridge isolated bidirectional dc–dc converter for high-frequency-link power-conversion system," *IEEE Transactions on Power Electronics*, vol. 29, no. 8, pp. 4091–4106, 2014.

[22] "Ieee standard for interconnection and interoperability of distributed energy resources with associated electric power systems interfaces," *IEEE Std 1547-2018*, pp. 1–138, 2018.

[23] N. Mohan, T. M. Undeland, and W. P. Robbins, *Power electronics: converters, applications, and design*. John wiley & sons, 2003.